ELSEVIER Nuclear Instruments and Methods in Physics Research A 467–468 (2001) 944–950

NUCLEAR INSTRUMENTS & METHODS IN PHYSICS RESEARCH Section A

www.elsevier.com/locate/nima

Parabolic refractive X-ray lenses: a breakthrough in X-ray optics

Bruno Lengeler[a,*], Christian G. Schroer[a], Boris Benner[a], Til Florian Günzler[a], Marion Kuhlmann[a], Johannes Tümmler[a], Alexandre S. Simionovici[b], Michael Drakopoulos[b], Anatoly Snigirev[b], Irina Snigireva[b]

[a] *II. Physikalisches Institut, Aachen University of Technology, D-52056 Aachen, Germany*
[b] *European Synchrotron Radiation Facility (ESRF), B.P. 220, F-38043 Grenoble Cedex, France*

Abstract

Refractive X-ray lenses, considered for a long time as unfeasible, have been realized with a rotational parabolic profile at our institute: The main features of the new lenses are: they focus in two directions and are free of spherical aberration. By varying the number of individual lenses in the stack the focal length can be chosen in a typical range from 0.5 to 2 m for photon energies between about 6 and 60 keV. The aperture of the lens is about 1 mm matching the angular divergence of undulator beams at 3d generation synchrotron radiation sources. They cope without problems with the heat load from the white beam of an undulator. Finally, they are easy to align and to operate. Refractive X-ray lenses can be used with hard X-rays in the same way as glass lenses can be used for visible light, if it is taken into account that the numerical aperture is small (of the order 10^{-4}). Being high-quality optical elements, the refractive X-ray lenses can be used for generating a focal spot in the μm range with a gain of a factor 1000 and more, or for imaging purposes as in a hard X-ray microscope. Recent examples from microanalysis, microtomography, fluorescence tomography, X-ray microscopy will be shown to demonstrate the state of the art. Possible new developments will be discussed.

PACS: 41.50; 07.85.T

Keywords: Refractive X-ray lenses; Hard X-ray microscope; Hard X-ray microbeam; Tomography; Spectroscopy; Synchrotron radiation instrumentation

1. Introduction

Refractive lenses for visible light, like glass lenses, are among the most versatile optical components. Their manufacture is easy because the index of refraction is appreciably larger than 1 (strong refraction) and absorption is weak. For hard X-rays, on the other hand, refraction in condensed matter is weak and absorption is strong. This becomes apparent in the index of refraction

$$n = 1 - \delta + i\beta \quad (1)$$

where the dispersive decrement δ is of the order 10^{-5}–10^{-7} and where β is related to the linear

*Corresponding author. Tel.: +49-241-807075; fax: +49-241-8888306.

E-mail address: lengeler@physik.rwth-aachen.de (B. Lengeler).

0168-9002/01/$ - see front matter
PII: S0168-9002(01)00531-9

absorption coefficient μ and to the photon wavelength λ by

$$\beta = \frac{\lambda\mu}{4\pi}. \quad (2)$$

At 1 Å wavelength (12.4 keV) $1/\mu$ in Al is 274 μm, illustrating the strong absorption of X-rays in matter. As a consequence, it has become textbook knowledge that there are no refractive lenses for X-rays. However, refraction of X-rays in matter is not zero and absorption is not infinite, and so refractive X-ray lenses with a focal length in the meter range should be feasible. Indeed, in 1996 [1] we have realized a first refractive X-ray lens. A number of holes, 1 mm in diameter and 4 mm deep, were well aligned in a piece of aluminum. The material left between the holes has concave shape and, hence, focuses the X-rays as expected when the real part of n is smaller than 1. The small refraction is compensated by aligning many holes in a stack. Absorption is minimized by choosing Al, or even better Be, as lens material, since the mass absorption coefficient decreases with the atomic number Z like Z^3. Although this procedure has clearly demonstrated the feasibility of refractive X-ray lenses [2–4], aligned holes in Al or Be do not perform in an optimized way. Spherical aberration blurs the focal spot and form fidelity and surface finish are hard to control. Therefore, we have designed and manufactured at the University of Technology in Aachen refractive X-ray lenses with a rotational parabolic profile (Fig. 1) [5–7]. The test of the lenses is done at ESRF in Grenoble. When the radius of curvature at the apex of the parabola is R, a stack of N lenses has a focal length

$$f = \frac{R}{2\delta N}. \quad (3)$$

Let us consider a typical example. At 20 keV, $N = 74$ aluminium lenses ($\delta = 1.355 \times 10^{-6}$, $R = 0.2$ mm) are needed to generate a focal length of 1 m. Aluminium lenses are manufactured by an embossing technique, similar to the minting of metallic coins. The accuracy of the punches must be in the μm range. The alignment of the optical axes of the individual lenses in a stack must also be done with an accuracy of 1 μm [7].

2. Optimizing of parabolic refractive lenses

We consider now the parameters which affect the quality of refractive X-ray lenses.

2.1. Low Z lens material

The transmission of a stack with N lenses is given by [7]

$$T = \exp(-\mu N d)[1 - \exp(-2a_p)]/2a_p \quad (4)$$

$$2a_p = \frac{\mu N R_0^2}{R} \sim (\mu/\rho)R_0^2/f. \quad (5)$$

Note that $(NR_0^2/R + Nd)$ is the length of the stack. For a given wavelength λ and a given focal length f, a_p depends only on the mass absorption

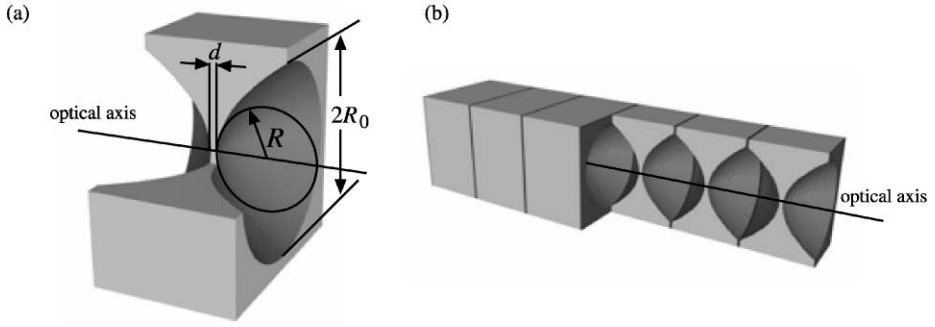

Fig. 1. (a) Individual refractive X-ray lens with parabolic profile, with radius of curvature R at the apex, and with geometrical aperture $2R_0$. (b) Stack of lenses forming a compound refractive lens.

coefficient μ/ρ and is independent of R and of ρ. Fig. 2 shows the energy dependence of μ/ρ for the light elements Li, Be, B, C, Al and for Ni. The advantage of low Z elements as lens material is obvious, since μ/ρ decreases with Z^3/E^3. However, Compton scattering starts to exceed photoabsorption below about $0.2\,\mathrm{cm}^2/\mathrm{g}$. Therefore, transmission is ultimately limited by Compton scattering. A Compton scattered photon does not contribute to focusing and, in addition, blurs the focal spot. In this sense Compton scattering is more detrimental than photoabsorption.

2.2. Small angle scattering

Besides photoabsorption and Compton scattering, focusing is hampered by small angle scattering. We have observed large differences in small angle scattering (more than 5 orders of magnitude) between different low Z compounds. Polymers which contain mixtures of amorphous and crystalline phases are not recommendable, nor are graphites appropriate when their density is appreciably below $2.26\,\mathrm{g/cm}^3$, so that they contain a high concentration of pores [4,7].

2.3. Machinabilty

Ductile materials like Al or Be (at elevated temperatures) can be processed by an embossing techniques. Hard material may be processed by grinding. In any case, the form fidelity is a critical parameter if the lenses should be used for imaging. The lens shape should agree with the rotational parabolic profile within 1 μm. This can be achieved as shown in Fig. 3.

A word should be said about the influence of roughness on a refractive lens. The lens of Fig. 3 shows an rms roughness σ of about 0.1 μm. This would be a very large value for an X-ray mirror but is not for a lens. The roughness σ enters into the transmission, effective aperture, and lateral resolution via the extended parameter

$$a_p = (R_0^2/2R^2)/(\mu NR + 2NQ_0^2\sigma^2). \tag{6}$$

For a lens the momentum transfer

$$Q_0 = k_1 - nk_1 = \delta k_1 \approx 10^{-5}\ \mathring{A}^{-1}. \tag{7}$$

For a mirror used at an angle θ_1 of 0.1°, the momentum transfer is

$$Q = 2k_1\theta_1 \approx 3 \times 10^{-2}\ \mathring{A}^{-1}. \tag{8}$$

For equal damping by roughness, the lens may tolerate a roughness that is a few thousand times larger than that for a mirror

$$\sigma_L = \sigma_M(Q/Q_0) = \sigma_M(2\theta_1/\delta) \approx 3000\sigma_M. \tag{9}$$

The low momentum transfer in a lens relieves the requirements for surface finish of refractive lenses

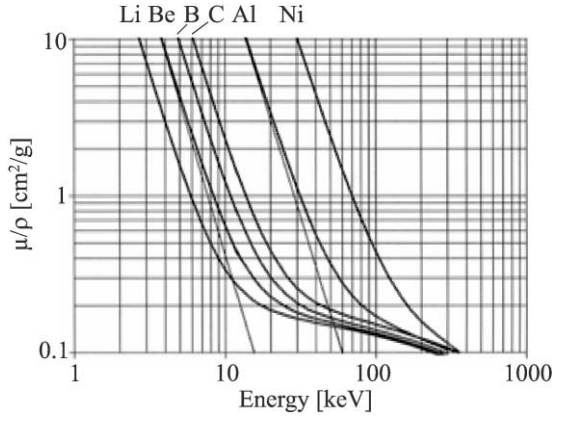

Fig. 2. Mass absorption coefficient μ/ρ for Li, Be, B, C, Al, and Ni. Below $0.2\,\mathrm{cm}^2/\mathrm{g}$ Compton scattering dominates the attenuation.

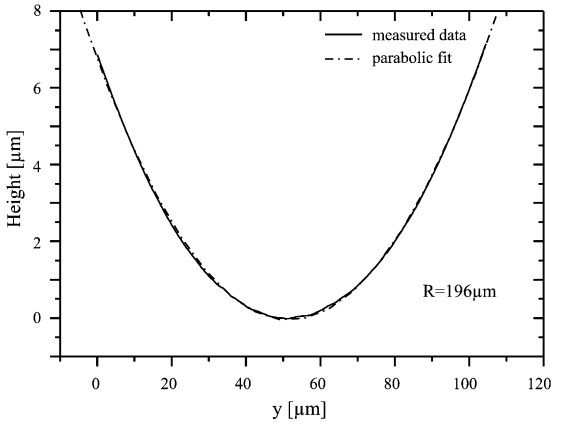

Fig. 3. Form fidelity of an Al refractive lens as measured by interferometry. The full line gives the measured profile and the broken line a fit with a parabola with $R = 196$ μm.

to such a degree that they can be manufactured in a standard laboratory environment.

2.4. Stability in X-ray beam

Stability in the X-ray beam is a prerequisite of any useful lens material. Metallic materials are excellently suited because X-rays are not able to displace atoms from their lattice site. On the other hand, most plastics and insulators deteriorate, either by the cracking of chemical bonds or by the generation of charged defects. For instance, a lens made out of polycarbonate ($C_{16}H_{14}O_3$) exposed for 10 h to a beam of 14.4 keV with 10^{12} ph/s/mm^{-2} deteriorates to such a degree that the image of the source, demagnified by the lens, increases in the vertical direction from 3.4 to 16.4 μm. This exposure corresponds to an absorbed energy dose of 9×10^6 Gy. The radiation damage is visible as a change in color. Other plastic materials, like Plexiglass (PMMA) deteriorate even much faster showing numerous blisters after 10 h exposure time.

For undulator beam lines at third generation synchrotron radiation sources the heat load on the first optical element may be a serious problem. We have tested an Al lens with 25 individual lenses in the white beam of an ESRF undulator (about 50 W/mm^2). In still air the temperature of the lens stabilizes at 150°C after 15 min. No deterioration of the lens performance was observed. In case of a higher heat load a water cooling of the lenses might be applied. We expect that Be or B lenses might even cope with the average heat load of a X-ray free electron laser (about 600 W/mm^2), since both Be and B have a lower absorption and a higher melting point than Al.

Fig. 4 shows a stack of individual lenses (with Al core) in their housing. The refractive X-ray lenses are very robust and easy to align in the beam. They have the size of a match box.

In the meantime, refractive X-ray lenses are widely considered as promising optical components for synchrotron radiation sources. A number of posters at this conference discuss different approaches for their manufacture, like spherical moulding in plastics (POS1-138), in metals (POS1-137), or air bubbles in a resin (POS1-130). At present, none of these lenses have a parabolic profile and their performance is inferior to that of the lenses presented in this paper.

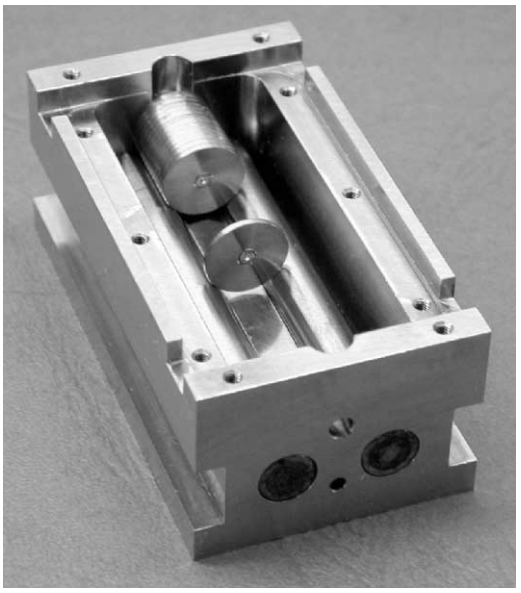

Fig. 4. Photograph of a refractive X-ray lens with parabolic profile in its housing (dimensions: 70 mm × 40 mm × 30 mm).

3. Applications of parabolic refractive X-ray lenses

3.1. Microfocus

There is an increasing demand for improving the lateral resolution of X-ray techniques, like diffraction, fluorescence, absorption and reflectivity. The parabolic refractive lenses are excellently suited for this purpose. Indeed, the lens demagnifies the source on the sample. In order to achieve a small spot size, the source size should be small, the source to lens distance L_1 should be large whereas the focal length f and the lens to detector distance L_2 should be small. The demagnification is

$$m = L_2/L_1 = f/(L_1 - f). \quad (10)$$

A demagnification by a factor 20–100 can be achieved. As an example we consider the undulator at beamline ID18 at the ESRF, which has a source size of 54×812 μm^2 full-width at

half-maximum (FWHM) in the vertical and in the horizontal. An aluminum lens with $N = 120$ and $L_1 = 58$ m has at 19.5 keV a focal length of 57 cm, and a demagnification of 1/102. We have detected 1.1×10^{10} ph/s in a focal spot of $0.55 \times 5.4\ \mu m^2$. There are 1020 times more photons in this spot size than in a pinhole of equal size.

A similar set-up was used to determine the dislocation density in individual grains of cold-rolled steel [8,9]. For this purpose eight Bragg reflections have been measured for each of a total of 45 grains. Strain generated by the rolling process broadens the Bragg reflections by generating a spread in the lattice parameter and by tilting the lattice planes against one another. It turns out that after a 25% deformation the dislocation density increases by a factor varying between 6 and 43 depending on the orientation of the grains, as compared to the value of non-deformed steel.

3.2. X-ray imaging

Parabolic refractive X-ray lenses have no spherical aberration and are therefore excellently suited for imaging purposes. An object is illuminated from the backside by synchrotron radiation. As in any microscope the object is located slightly outside of the focal distance of the refractive lens. This results in a strong magnification $m = L_2/L_1$. Fig. 5 shows a micrograph of a gold mesh. Superposed to a square mesh with 15 μm period is a linear mesh with 1 μm period. An Al lens with $N = 100$ and a focal length of 109 cm at 25 keV is at a distance of 114 cm from the object. The image at $L_2 = 22.38$ m is magnified by a factor of 20. It is noteworthy that this hard X-ray microscope is able to image opaque objects. The lines of the linear grid are visible behind the bars of the quadratic grid. This implies little sample preparation and even allows for in situ studies of delicate samples such as, e.g., biological objects in their natural environment. The field of view of the microscope is between 300 and 500 μm. Note that some flaws in the linear Au grid are clearly visible.

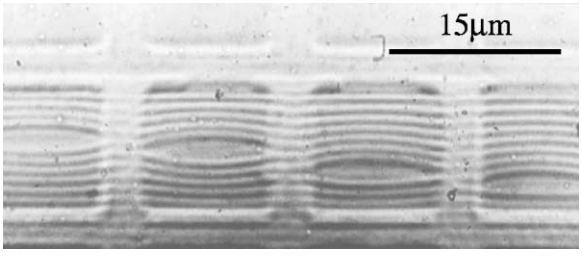

Fig. 5. X-ray micrograph of a Au mesh (with a square period of 15 μm and a linear period of 1 μm) taken with an Al refractive lens at 19 keV. The magnification is 22 times. Some flaws in the linear array are visible.

The lateral resolution of the microscope is given by

$$d_t = 0.75\frac{\lambda}{2NA} = 0.75\lambda\frac{L_1}{D_{eff}}, \tag{11}$$

$$D_{eff} = 2R_0\sqrt{(1 - \exp(-a_p))/a_p}. \tag{12}$$

Absorption (and to a smaller extend roughness) reduce the effective aperture D_{eff} compared to the geometric aperture $2R_0$. As outlined above, Compton scattering ultimately limits the resolution of the lens. Up to now, we have achieved a lateral resolution of 300 nm. Using Be or B as lens material a lateral resolution of 80 nm can be expected. The longitudinal resolution is given by

$$d_l = 0.64\frac{\lambda}{(NA)^2}. \tag{13}$$

The numerical aperture NA being small (of the order 10^{-4}), the longitudinal resolution is about 1 cm. This implies that the 3d structure of an object, has to be reconstructed by tomography.

Photoabsorption is a common way to generate contrast in microscopy. However, in X-ray microscopy phase contrast might be much more favorable. Indeed, the ratio δ/β of the dispersive and absorptive contributions in the index of refraction varies as E^3/Z^3. In other words, for low Z elements at high energies phase contrast is more favorable. As an example, for boron at 16 keV the ratio $\delta/\beta = 2800$. Fig. 6 shows an image of the antenna of an insect detected in projection geometry ($m = 1$) and by means of a refractive lens with 0.5 μm resolution and 18 times magnification at 23.3 keV. Two points are noteworthy. This object is completely transparent for 23.3 keV photons, i.e., absorption does not contribute to the contrast. The phase contrast, however, is clearly

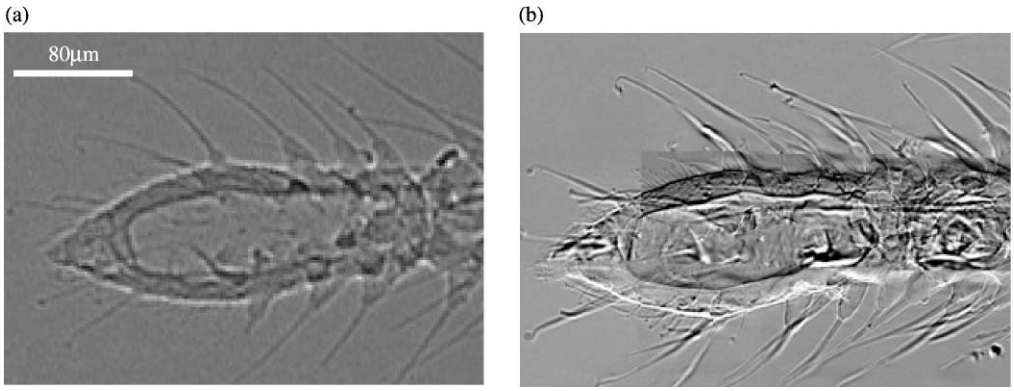

Fig. 6. Antenna of an insect detected at 23.3 keV in projection geometry (a) and with a refractive Al lens (b) ($m = 18$).

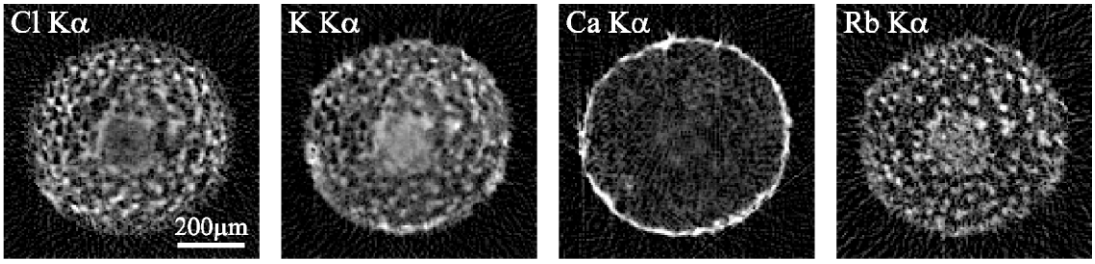

Fig. 7. Fluorescence microtomography of a mahogany root detected with Al refractive lens at 19.5 keV. The distribution of Cl, Ca, K, and Rb in a virtual cross section of the root is shown.

visible at the cilia as interference fringes. Secondly, many more details are visible with the microscope than in pure projection.

3.3. Combination of imaging and spectroscopy

A hard X-ray microscope opens the possibility to combine imaging with spectroscopy, as for instance fluorescence spectroscopy. By rotating and translating the sample in a microbeam and by detecting at the same time the fluorescence radiation in an energy dispersive detector, the distribution of different atomic species can be determined by tomographic reconstruction. This might be of interest for studying the metabolism in plants, as illustrated in Fig. 7. The distribution of Cl, Ca, K und Rb in the root of a mahogany plant (*Swietenia macrophylla*) is determined with 6 μm resolution. Rubidium occurs naturally as companion of potassium. Although the concentration is only 3×10^{-3} of that of K it can nevertheless be identified without problems because its fluorescence photons are much easier to be detected than those of K.

4. Conclusion

We have developed parabolic refractive X-ray lenses. They are genuine X-ray optical components, like glass lenses for visible light. However, the numerical aperture is small (of the order 10^{-4}). The new lenses are mechanically robust, easy to align in the beam (in about 15 min) and thermally stable. The energy range of application is 12–60 keV for Al lenses and 2–50 keV for Be and B lenses. For 100 keV Ni lenses seem to be appropriate. The focal length is in the meter range. They

are easily tunable by changing the number N of lenses in the stack. A microbeam in the μm range and below with 10^{10} ph/s/μm^2 has been achieved. A hard X-ray microscope for opaque objects requiring little sample preparation has been realized. The lateral resolution can be as low as 80 nm. Refractive X-ray lenses are also interesting optical components for X-ray tubes.

References

[1] A. Snigirev, V. Kohn, I. Snigireva, B. Lengeler, Nature 384 (1996) 49.
[2] A. Snigirev, V. Kohn, I. Snigireva, A. Souvorov, B. Lengeler, Appl. Opt. 37 (4) (1998) 653.
[3] A. Snigirev, B. Filseth, P. Elleaume, T. Klocke, V. Kohn, B. Lengeler, I. Snigireva, A. Souvorov, J. Tümmler, in: A.M.K.A.T. Macrander (Ed.), High Heat Flux and Synchrotron Radiation Beamlines, Proceedings of the SPIE, Vol. 3151, Bellingham, WA, 1997.
[4] B. Lengeler, J. Tümmler, A. Snigirev, I. Snigireva, C. Raven, J. Appl. Phys. 84 (11) (1998) 5855.
[5] B. Lengeler, C.G. Schroer, M. Richwin, J. Tümmler, M. Drakopoulos, A. Snigirev, I. Snigireva, Appl. Phys. Lett. 74 (26) (1999) 3924.
[6] B. Lengeler, C.G. Schroer, J. Tümmler, B. Benner, M. Richwin, A. Snigirev, I. Snigireva, M. Drakopoulos, Synchrotron Radiat. News 12 (5) (1999) 45.
[7] B. Lengeler, C. Schroer, J. Tümmler, B. Benner, M. Richwin, A. Snigirev, I. Snigireva, M. Drakopoulos, J. Synchrotron Radiat. 6 (1999) 1153.
[8] O. Castelnau, T. Ungar, M. Drakopoulos, A. Snigirev, I. Snigireva, C. Schroer, T. Chauveau, B. Bacroix, Key Engineering Materials, Vol. 177–180, Trans Tech Publications, Ütikon a.s., Switzerland, 2000.
[9] M. Drakopoulos, I. Snigireva, A. Snigirev, O. Castelnau, T. Chauveau, B. Bacroix, C.G. Schroer, T. Ungar, in: W. Meyer-Ilse, T. Warwick, D. Attwood (Eds.), X-Ray Microscopy: Proceedings of the Sixth International Conference, AIP Conference Proceedings, Vol. 507, American Institute of Physics, Melville, NY, 2000.